The crystal structure of Pyrococcus abyssi tRNA (uracil-54, C5)-methyltransferase provides insights into its tRNA specificity

Hélène Walbott, Nicolas Leulliot, Henri Grosjean, Béatrice Golinelli-Pimpaneau

Published online 24 July 2008

Nucleic Acids Research, 2008, Vol. 36, No. 15 ***4929–4940***
doi:10.1093/nar/gkn437

The crystal structure of *Pyrococcus abyssi* tRNA (uracil-54, C5)-methyltransferase provides insights into its tRNA specificity

Hélène Walbott[1], Nicolas Leulliot[2], Henri Grosjean[1] and Béatrice Golinelli-Pimpaneau[1,*]

[1]Enzymology and Structural Biochemistry Laboratory, CNRS, 1 avenue de la Terrasse, 91198 Gif-sur-Yvette and [2]Institute of Molecular and Cellular Biochemistry and Biophysics, University Paris-South 11, 91400 Orsay, France

Received April 2, 2008; Revised May 25, 2008; Accepted June 25, 2008

ABSTRACT

The 5-methyluridine is invariably found at position 54 in the TΨC loop of tRNAs of most organisms. In *Pyrococcus abyssi*, its formation is catalyzed by the S-adenosyl-L-methionine-dependent tRNA (uracil-54, C5)-methyltransferase ($_{Pab}$TrmU54), an enzyme that emerged through an ancient horizontal transfer of an RNA (uracil, C5)-methyltransferase-like gene from bacteria to archaea. The crystal structure of $_{Pab}$TrmU54 in complex with S-adenosyl-L-homocysteine at 1.9 Å resolution shows the protein organized into three domains like *Escherichia coli* RumA, which catalyzes the same reaction at position 1939 of 23S rRNA. A positively charged groove at the interface between the three domains probably locates part of the tRNA-binding site of $_{Pab}$TrmU54. We show that a mini-tRNA lacking both the D and anticodon stem-loops is recognized by $_{Pab}$TrmU54. These results were used to model yeast tRNA^{Asp} in the $_{Pab}$TrmU54 structure to get further insights into the different RNA specificities of RumA and $_{Pab}$TrmU54. Interestingly, the presence of two flexible loops in the central domain, unique to $_{Pab}$TrmU54, may explain the different substrate selectivities of both enzymes. We also predict that a large TΨC loop conformational change has to occur for the flipping of the target uridine into the $_{Pab}$TrmU54 active site during catalysis.

INTRODUCTION

In all organisms, numerous highly specific modification enzymes are involved in the posttranscriptional maturation of various types of RNAs. Determining the 3D structure of these enzymes may allow to get insights into how they specifically recognize their RNA substrates. Among the 107 chemically different nucleoside modifications found in RNAs, 91 are found in tRNA (1) (http://medlib.med.utah.edu/RNAmods). While modifications in the anticodon region of tRNA are important for translation fidelity (2), the functions of other modifications are less well characterized. Some of them can have an important role in the correct folding of tRNA (3) and final stabilization of the tRNA tertiary structure, as well as in the recognition and discrimination of tRNA by the cognate aminoacyl-tRNA synthetase and translation factors (4).

The methylations at different base positions and at the 2′ hydroxyl group of ribose are the most frequently encountered modifications. Among them, the methylation of uridine to 5-methyluridine (or ribothymidine, m^5U) is a common modification found in both tRNA and rRNA. In *Escherichia coli*, m^5U is found at two conserved positions, 1939 or 747, of 23S rRNA, its formation being catalyzed by the methyltransferases (MTases) RumA and RumB (5,6), respectively. m^5U is also present at position 54 in the TΨC loop in almost all tRNAs from bacteria and eukarya, and two S-adenosyl-L-methionine (AdoMet)-dependent enzymes catalyzing this modification have been identified, TrmA in *E. coli* (7) and Trm2p in the yeast *Saccharomyces cerevisiae* (8). RumA, RumB, TrmA and Trm2p all belong to the same family of AdoMet-dependent RNA (Uracil, C5)-MTases (Cluster of Orthologous Group COG2265), suggesting that they derive from a single common ancestor (9). Since some bacterial genomes contain multiple genes of the RumA/RumB/TrmA/Trm2p family coding for either tRNA or rRNA MTases, it is probable that duplication events, followed by changes in target specificity, occurred during evolution.

Proteins of the RumA/RumB/TrmA/Trm2p family are generally organized in three domains (10). The C-terminal catalytic domain displays the typical AdoMet-dependent MTase Rossmann-like fold. The central domain usually

*To whom correspondence should be addressed. Tel: 33 1 69 82 42 35; Fax: 33 1 69 82 31 29; Email: beatrice.golinelli@lebs.cnrs-gif.fr
Present addresses:
Hélène Walbott, Institute of Molecular and Cellular Biochemistry and Biophysics, University Paris-South 11, 91400 Orsay, France
Henri Grosjean, Institute of Genetics and Microbiology, University Paris-South 11, 91400 Orsay, France

contains a [Fe_4S_4] cluster, which was proposed to be essential for the structural integrity of RumA (11). The N-terminal TRAM domain, common to tRNA uracil methylation and 2-methyladenine thiolation enzymes, is predicted to be an RNA-binding domain (9). However, homologs of the TrmA and RumB proteins lack the N-terminal TRAM domain and some members of the RumA/RumB/TrmA/Trm2p family also seem to lack the cysteines involved in the [Fe_4S_4] cluster (10). The catalytic and substrate specificity of RumA and TrmA have been studied (5,11–13). Moreover, the structure of RumA has been determined alone (14) and in complex with S-adenosyl-L-homocysteine (AdoHCys) and a covalently bound 37-mer fragment of rRNA containing 5-fluorouridine (5FU) at the position of modification (14).

In contrast to eukaryotes and bacteria, m^5U54 is rarely present in tRNAs from archaea. We have recently identified the gene coding for the AdoMet-dependent tRNA (uracil-54, C5) MTase in the archaeal *Pyrococcus abyssi*, purified and characterized the corresponding recombinant protein, $_{Pab}$TrmU54 (10). We have shown that the protein purified under aerobic conditions is specific for tRNA but not rRNA, and specifically modifies the U54 position in the TΨC loop of yeast $tRNA^{Asp}$ (10). Although sequence analysis predicted that $_{Pab}$TrmU54 possesses a C-terminal catalytic domain and a [Fe_4S_4] cluster containing central domain, the presence of the N-terminal TRAM domain was unclear. Unexpectedly, detailed phylogenetic sequence analysis of RumA homologs has shown that $_{Pab}$TrmU54 is closer to RumA (acting on rRNA) than to Trm2p or TrmA (acting on tRNA) (10). We have thus proposed that the gene encoding $_{Pab}$TrmU54 was acquired during evolution by the common ancestor of Thermococcales and Nanoarchaea via a single horizontal gene transfer of a RumA-type sequence from a bacterial donor. Since $_{Pab}$TrmU54 appears to have diverged from RumA much less than the other tRNA MTases TrmA and Trm2p (10), it is an ideal model to study how the RNA specificity of a MTase that methylates the C5 position of uridine has evolved.

In order to investigate the molecular basis for the tRNA specificity of $_{Pab}$TrmU54, we have determined its crystal structure in complex with AdoHCys at 1.9 Å resolution. Comparison of the $_{Pab}$TrmU54 and RumA·AdoHCys·mini-rRNA structures (15) reveals a similar overall domain organization. Moreover, we show that a tRNA lacking both the D and anticodon stem-loops is recognized by $_{Pab}$TrmU54. This allows us to propose a model of the $_{Pab}$TrmU54·tRNA complex, in which the aminoacyl acceptor stem of tRNA is bound by the TRAM domain and the TΨC loop is in proximity of the catalytic site. This model highlights essential differences in the loops involved in RNA binding in $_{Pab}$TrmU54 compared with RumA.

MATERIAL AND METHODS

Protein preparation, purification and crystallization

Form I of recombinant $_{Pab}m^5U54$, tagged with six histidines at the N-terminus, was purified as described previously (10). The protocol was modified as follows for Form II of the native protein and for the selenomethionylated protein. Bacteria were grown in 1l MM9 minimal medium (Difco Voigt Global Distribution Inc., Lawrence, KS, USA) supplemented with 1 mM $MgSO_4$, 0.3 mM $CaCl_2$, 0.5% glucose, 1 μg/l thiamin, 30 μg/ml chloramphenicol and 50 μg/ml kanamycin. After growth at 37°C to an OD_{600} of 0.6–0.8, the L-amino acids lysine, leucine, threonine and phenylalanine at 100 mg/l, valine and isoleucine at 50 mg/l, as well as selenomethionine (Calbiochem, Merck KGaA, Darmstadt, Germany) or methionine for Form II of the native protein at 60 mg/l were added to inhibit the methionine pathway. After 30 min at 37°C, expression was induced at 20°C by addition of isopropyl-β-D-thiogalactopyranoside to a final concentration of 1 mM. Cells were collected by centrifugation after overnight incubation. All the proteins were purified using Ni^{2+} affinity (10) and concentrated to 8.3 mg/ml in 50 mM sodium phosphate pH 8, 300 mM NaCl, 250 mM imidazole, 5 mM EDTA, 2 mM DTT using a centricon YM-10 membrane (Amicon Millipore Corporation, Billerica, MA, USA). Crystals were grown at 18°C in hanging-drops by vapor diffusion. 1 μl of a mixture of protein and AdoMet in a 1:2 molar ratio was added to 1 μl of a 0.6 ml reservoir solution (15% PEG 8000, 0.05 M ammonium sulfate, 0.1 M sodium citrate pH 5.6). Crystals grew to a size of 0.02 mm × 0.02 mm × 0.01 mm for Form I or 0.1 mm × 0.02 mm × 0.01 mm for Form II in a few days. Crystals were transferred stepwise from the crystallization solution to the same solution containing 25% glycerol and were flash frozen in a cold nitrogen stream at 100K.

X-ray data collection structure determination and refinement

Diffraction data were collected at the European Synchrotron Radiation Facility in Grenoble on beamline ID14EH2 for Form I, ID23EH1 for Form II and BM30A for the three MAD datasets of the selenomethionylated Form II. Data were processed with *MOSFLM* and *SCALA* (16) (Table 1). Despite the structural similarity of RumA and $_{Pab}$TrmU54, attempts to solve the $_{Pab}$TrmU54 structure by molecular replacement have remained unsuccessful. Therefore, the structure was solved by MAD using a crystal of the selenomethylated protein. The seven selenium sites of $_{Pab}$TrmU54 were initially located with *SHELXC/D* (17) with the dataset collected at the peak wavelength. Phases were determined in *AUTOSHARP* (18) using the three MAD datasets and improved upon solvent flattening with *SOLOMON* (19). Automatic model building with *ARP/WARP* (20) allowed to trace 90% of the residues in the native dataset, *O* (21) and *COOT* (22) were used for final model building. Refinement was carried out with *REFMAC5* (23). The structure of Form I of the native protein was solved by molecular replacement with *MOLREP* (24) using the Form II structure. Structures validation was done with *MOLPROBITY* (25). The final models of Forms I and II (accession numbers are present in Appendix 1) contain 392 and 398 residues out of 405, respectively. There was no electron density for several residues of the histidine tag or in the central domain corresponding to the

Table 1. Data collection and refinement statistics

	Native		SeMet		
	Form I	Form II	Form II		
Data collection					
Space group	$P2_12_12_1$	C2	C2		
Cell dimensions *a*, *b*, *c* (Å)	63, 63.5, 102.1	99.5, 100.4, 55.7	99.9, 99.8, 55.5		
α, β, γ (°)	90, 90, 90	90, 111.6, 90	90, 111.4, 90		
			Peak	Inflection	Remote
Wavelength (Å)	0.933	1.28215	0.98013	0.98044	0.90001
Resolution (Å)	30–1.9	68–2.1	30–3		
Outer resolution shell (Å)	1.93–1.9	2.21–2.1	3.16–3		
Number of observed reflections/ unique	173 151/33 008	105 494/28 990	35 623/10 263	42 192/10 173	39 304/10 188
Completeness (%) (outer shell)	99.7 (98.5)	97.4 (96.4)	99.6 (97.7)	99.6 (98.3)	99.9 (100)
Redondance (outer shell)	5.2 (4.9)	3.6 (3.7)	3.5 (2.3)	4.1 (2.7)	3.9 (3.9)
I/σ (I) (outer shell)	22 (3.7)	19 (3)	19.4 (3.1)	22.0 (4)	20.8 (4.7)
R_{merge} (%) (outer shell)	7.2 (47.6)	5.2 (40.5)	5.7 (24.5)	5.8 (19.5)	5.8 (20.7)
MAD phasing			Ano	Iso/ano	Iso/ano
R_{cullis} (acentric) (%)			85.6	59.2/90.8	47.5/88.7
Phasing power (acentric)			0.98	0.51/0.85	0.24/0.84
Figure of merit			0.38		
Refinement					
Resolution (Å)	20–1.9	20–2.1			
R/R_{free} (%)	20.5/24.1	21.1/25.4			
RMSD					
Bond lengths (Å)	0.009	0.011			
Bond angles (°)	1.184	1.358			
B-factors (Å^2)	22.4	34.9			
Protein (global)	21.3	34.7			
TRAM domain	37.4	39.6			
Central domain	21.4	30.7			
Ccatalytic domain	17.0	36.8			
AdoHCys	19.6	31.6			
Water	33.4	39.9			
Ramachandran statistics (%)					
Favored	99.0	97.4			
Allowed	1.0	2.6			

iron–sulfur-binding site, which are disordered. The model includes residues Met1-Val57, Gly69-Glu124, Lys127-Val405 for Form I whereas that for Form II has three additional residues both at the N-terminus and in the iron–sulfur-binding site. Superposition of the structures has been made with *SUPERPK* (P. Alzari, personal communication) and *LSQKAB* (26).

Formation of the 5FU-mini-tRNA·$_{Pab}$TrmU54 complex

The formation of the 5FU-mini-tRNA·enzyme covalent complex was analyzed on a 10% denaturating acrylamide gel. Enzyme (9 μM) was incubated for 2 h at 50°C with 5FU-mini-tRNA (36 μM) and AdoMet (100 μM) in 25 mM sodium phosphate pH 7.2, 25 mM KCl, 5 mM $MgCl_2$, 2 mM DTT, 5% glycerol.

RESULTS AND DISCUSSION

Overall structure of $_{Pab}$TrmU54

Two different crystal forms (I and II) of $_{Pab}$TrmU54 in complex with AdoHCys, belonging to space groups $P2_12_12_1$ and C2, respectively, and containing one molecule in the asymmetric unit, were obtained (data collection statistics are reported in Table 1). The structure of Form II was determined by MAD, using a single crystal of the selenomethionylated protein and used as a model for solving the structure of Form I by molecular replacement. The two structures are nearly identical with a r.m.s.d. of 0.7 Å on the whole molecule, as determined with the *DaliLite* server (27).

Like RumA, the protein is organized into three different domains (Figure 1A). Superpositions of the $_{Pab}$TrmU54 structure with the RumA·AdoHCys·mini-rRNA and RumA structures with *DaliLite* indicate r.m.s.d. of 2.3 or 2.4 Å and *Z*-scores of 37.6 or 37.5, for 372 aligned Cαs, respectively (Figure 1B). Therefore, despite the low amino acid sequence identity (23%) between $_{Pab}$TrmU54 and RumA, the 3D structures are essentially similar.

The N-terminal domain is a TRAM domain

The presence of a TRAM domain in $_{Pab}$TrmU54 was not detected using domain data bases such as *InterPro*, *Pfam* or *PROSITE* and it was not directly apparent from the sequence comparison with RumA (Figure S1) since the $_{Pab}$TrmU54 N-terminal and RumA TRAM domains display only 20% sequence identity (10). The $_{Pab}$TrmU54 structure confirms that the N-terminal domain is a TRAM domain, which adopts the same five-stranded

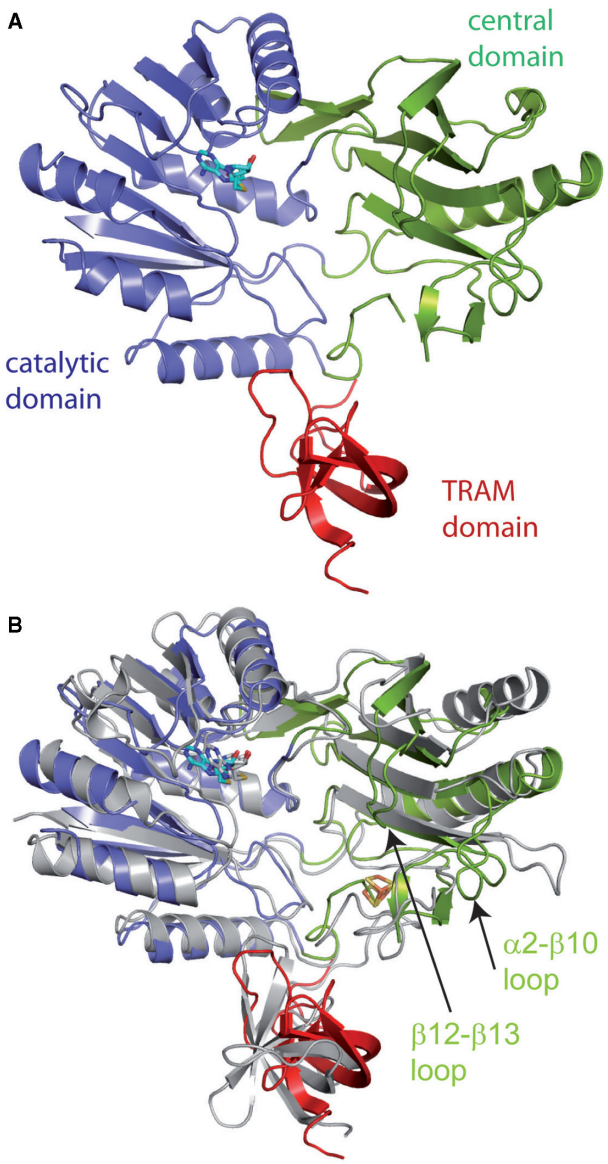

Figure 1. Structure of the $_{Pab}$TrmU54·AdoHCys complex and comparison to the RumA structure. (**A**) General view of the $_{Pab}$TrmU54·AdoHCys complex. The N-terminal TRAM domain is colored red, the C-terminal catalytic domain blue and the central domain green. AdoHCys is indicated in cyan stick representation. The catalytic domain of $_{Pab}$TrmU54 displays the class I AdoMet-dependent MTase fold with an additional β-strand that increases the connection between the catalytic and central domains. (**B**) Superposition of the $_{Pab}$TrmU54 and RumA structures. The structures of $_{Pab}$TrmU54 (same orientation and color code as in A) and RumA (in grey) were superimposed on the catalytic domains with *DaliLite* (r.m.s.d. of 1.8 Å and *Z*-score of 23.3 for 186 aligned Cαs). The AdoHCys and iron–sulfur cluster of RumA are shown in grey and yellow stick representations, respectively. Two extended loops of similar size, α2–β10 and β12–β13, are characteristic of $_{Pab}$TrmU54 and homologs of other Thermococcales organisms (Figure S1), whereas the corresponding loops are much shorter in RumA. All figures were drawn with PYMOL (http://www.pymol.org).

beta barrel architecture characteristic of an oligosaccharide/oligonucleotide-binding fold (OB-fold) (28) found in different nucleic acid-binding proteins (29). Superposition of the TRAM domains of RumA and $_{Pab}$TrmU54 with *DaliLite* gives a r.m.s.d. of 2.3 Å and a *Z*-score of 6.7 for 49 aligned Cαs. The main structural difference resides in loops β2–β3 and β4–β5, which, in $_{Pab}$TrmU54, are shorter and adopt different conformations compared with RumA (Figures 2 and S1). The corresponding loops interact with RNA in the RumA·mini-rRNA complex (see below).

The central domain is structured despite the absence of the iron–sulfur cluster

The central domain (residues 51–72 and 105–249) is the least conserved domain between proteins of the RumA-family (10) and the sequence identity for this domain in RumA and $_{Pab}$TrmU54 is 18%. In both enzymes, this domain adopts the same fold, consisting in a six-stranded β-sheet combined with three helices (r.m.s.d. of 2.3 Å and *Z*-score of 13.3 for 135 aligned Cαs). However, two extended loops of similar size, α2–β10 (residues 159–171) and β12–β13 (residues 213–224) are characteristic of $_{Pab}$TrmU54 and homologs of other Thermococcales organisms (Figures 1 and S1) whereas the corresponding loops are much shorter in RumA (residues 183–188 and 236–237, respectively).

In the central domain of RumA, a $[Fe_4S_4]$-binding pocket is formed by an extended loop β5–α1 containing three cysteines and a loop β9–α2 containing the fourth one (Figure S1). The central domain of $_{Pab}$TrmU54 also contains these four conserved cysteine residues that are presumed to coordinate an iron–sulfur cluster (Figure S1). Although the brownish coloration and the UV-visible absorption spectrum of $_{Pab}$TrmU54 right after purification on nickel affinity column under aerobic conditions indicated the presence of the $[Fe_4S_4]$ cluster [Figure 8 in (10)], the latter is not visible in the electron density in our structures. In fact, in the Form I structure, 13 residues corresponding to the iron–sulfur cluster-binding site of RumA (residues 58–68 in the β5–α1 loop and 125–126) were not observed in the electron density, indicating their disorder. In the Form II structure, 10 residues in this region are also lacking and two conserved cysteines out of the four form a disulfide bridge (data not shown). The absence of a characteristic signal in the emission fluorescence spectrum around the iron edge collected on one crystal (data not shown) confirms that the iron is not present in the $_{Pab}$TrmU54 structures.

According to mutagenesis experiments (14) and to the RumA·AdoHCys·mini-rRNA crystal structure (15), it has been shown that the iron–sulfur cluster of RumA is involved in the correct folding and the structure stabilization of the protein, as well as in RNA binding through water-mediated hydrogen bonds. The cluster was proposed to regulate the stability and/or function of the protein in response to changes in cellular environment. Yet, the requirement of the cluster in the catalytic mechanism is unlikely because the cluster is absent both in Trm2p and TrmA (Figure S1). Since the structures of the central domains of $_{Pab}$TrmU54 and RumA are highly similar, the reported structure of the $_{Pab}$TrmU54 central domain is likely not compromised other than locally by the absence of the cluster. The precise function of the iron–sulfur cluster still remains to be determined.

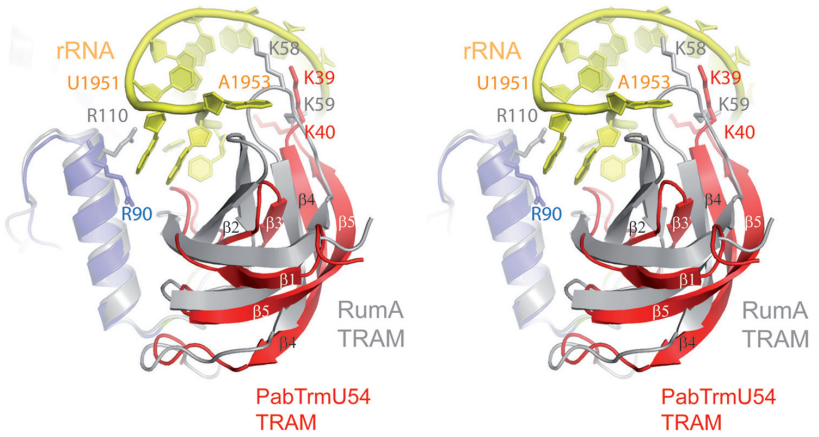

Figure 2. Comparison of the TRAM domains of $_{Pab}$TrmU54 and RumA. In the superposition of the TRAM domains of $_{Pab}$TrmU54 and RumA, the color scheme for $_{Pab}$TrmU54 is as in Figure 1. Residues important for RNA binding are shown in stick representation. The mini rRNA substrate of RumA is shown in yellow cartoons. The loops β2–β3 and β4–β5 in $_{Pab}$TrmU54 are shorter and adopt different conformations compared with RumA. Like in RumA, an RNA double helix may be bound by $_{Pab}$TrmU54 through the lysine residues K39 and K40 from loop β4–β5 and R90 from the catalytic domain.

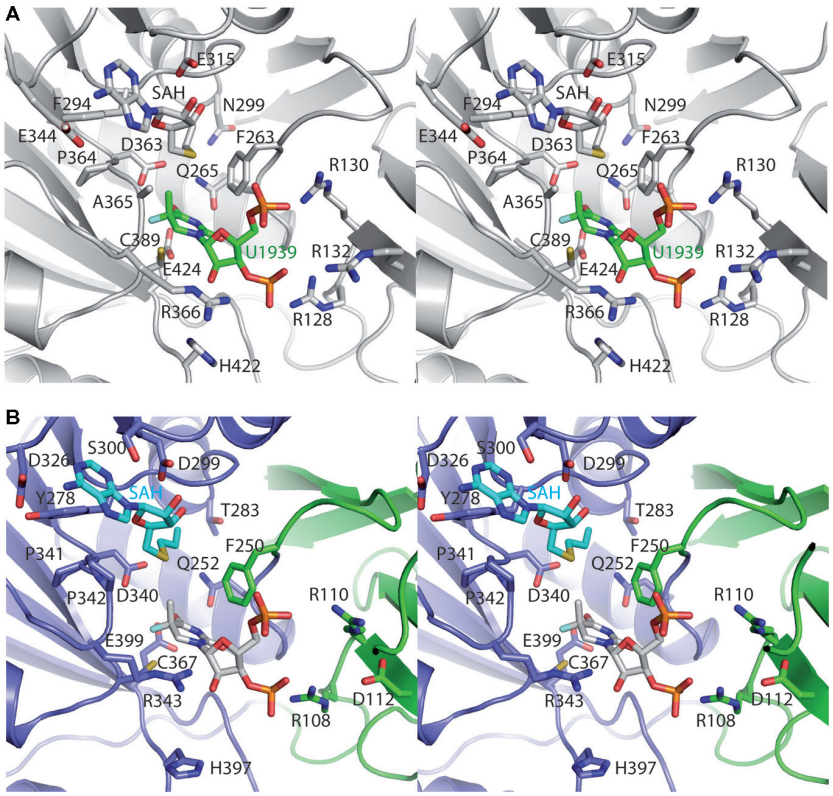

Figure 3. Detailed comparison of the $_{Pab}$TrmU54 and RumA catalytic sites. (**A**) Stereo view of the catalytic site of RumA. AdoHCys and the target uridine are shown in grey and green stick representations, respectively. (**B**) Stereo view of the catalytic site of $_{Pab}$TrmU54. The catalytic site of $_{Pab}$TrmU54 (same color code as Figure 1) is shown in the same orientation as that of RumA in A. The target uridine, as seen in the RumA·AdoHCys·mini-rRNA structure, and AdoHCys are shown in grey and cyan stick representations, respectively.

The catalytic domain adopts a classical Rossmann-like fold

Like in RumA, the C-terminal catalytic domain (residues 250–405) of $_{Pab}$TrmU54 displays the class I AdoMet-dependent MTase fold (30) with an additional segment composed of α1 and β6 (residues 73–104) that strongly reinforces the connection between the central and catalytic domains (Figure 1). AdoHCys is present in the catalytic site and has the same extended conformation as in RumA (Figure 3), with the same environment as in most AdoMet-dependent MTases (30). The exocyclic amino group and N1 atom of the adenine moiety of AdoHCys form H-bonds, with the carboxylate group and the backbone amide of D326, respectively.

The adenine ring of AdoHCys makes van der Waals and hydrophobic interactions with residues S300 and Y278. The sugar ring of AdoHCys stacks on P342 whereas its two oxygen atoms form H-bonds with the carboxylate group of D299. The terminal carboxylate of the homocysteine moiety is hydrogen bonded to the hydroxyl group of T283 and the amide side chain of Q252. While AdoHCys has been found in two different conformations in DNA MTases (31), the extended conformation, which is adopted by AdoMet in all structures of MTases, is catalytically active because the homocysteine moiety does not occupy the target base-binding pocket like in the other folded conformation.

Comparison of different (DNA cytosyl, RNA cytosyl and RNA uracil, C5)-MTase sequences (14) indicates that they contain 6 out of 10 conserved motifs that are potentially present in the Rossmann-like fold of the AdoMet-dependent MTases (30). It is likely that motifs IV, VI, VIII and X (Figure S1) have key roles in the specific binding of RNA or DNA, as well as for targeting uridine or cytosine (14). Mechanistic and mutagenesis studies of TrmA (12,13) and RumA (15) have addressed the function of several conserved residues located in the active site, as defined by the RumA·AdoHCys·mini-rRNA structure. In RumA, the reaction occurs through the nucleophilic attack of C389 of motif VI (C367 in $_{Pab}$TrmU54) on C6 of uridine to form a covalent enolate intermediate that activates C5 for methylation by AdoMet. The conserved glutamate E424 (E399 in $_{Pab}$TrmU54) of motif VIII acts as the general base in the following deprotonation of C5 of uridine. The conserved Q265 in motif X (Q252 in $_{Pab}$TrmU54) is involved in the specific recognition of U1939 via bidentate hydrogen bonds to N3 and O4 of the nucleotide and in AdoMet binding. The conserved F263 in the same motif (F250 in $_{Pab}$TrmU54) makes an edge-to-face stacking interaction with the target uridine base and contacts the homocysteine moiety of AdoHCys. P364 in motif IV (P341 in $_{Pab}$TrmU54) was proposed to promote product release by clashing with the transferred methyl group. The preceding aspartate D363 (D340 in $_{Pab}$TrmU54) contributes to the binding of the cofactor, orientates Q265 of motif X (Q252 in $_{Pab}$TrmU54) and stabilizes the enolate intermediate (15). R366 (R343 in $_{Pab}$TrmU54) forms H-bonds with both ribose oxygens of the target uridine. Since all the AdoMet-binding and catalytic residues are conserved in RumA and $_{Pab}$TrmU54 (Figures 3 and S1), the target uridine is likely similarly recognized by the two enzymes. Thus, the conformation of the target uridine in the $_{Pab}$TrmU54 catalytic site can be inferred from the RumA·AdoHCys·mini-rRNA structure, which provides important constraints for recognition of the tRNA by $_{Pab}$TrmU54 (see below).

The $_{Pab}$TrmU54 tRNA-binding site is located at the interface of the three domains

The 37-mer rRNA fragment in the RumA·AdoHCys·mini-rRNA complex is bound at the interface between the three domains of RumA (15) (Figure 4A). Similarly, in $_{Pab}$TrmU54, a narrow groove is formed at the interface between the central and the catalytic domains. This region is positively charged (except for a negatively charged region in the catalytic domain that forms the binding site of the positively charged AdoMet cofactor), as indicated by the electrostatic potential surface (Figure 4B), and likely accommodates the negatively charged tRNA. Since in the RumA·AdoHCys·mini-rRNA structure, the TRAM domain binds rRNA, part of tRNA in $_{Pab}$TrmU54 is also likely bound by the TRAM domain, which is more positively charged than that of RumA (Figure 4A and B). Therefore, the tRNA-binding site is probably formed at the interface between the three domains of $_{Pab}$TrmU54.

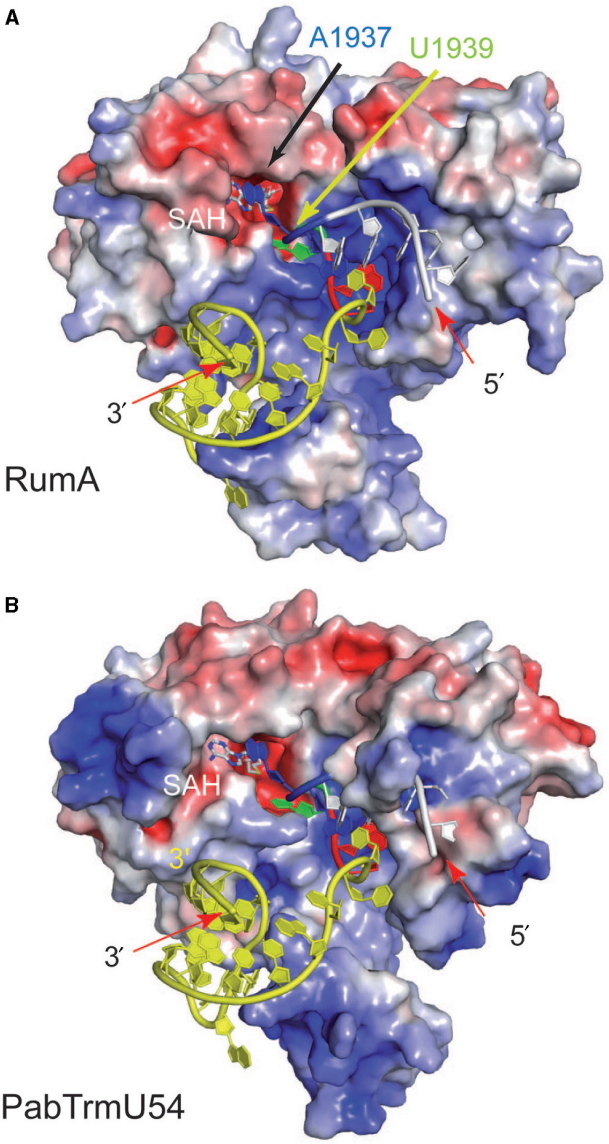

Figure 4. Comparison of the electrostatic potential surfaces of $_{Pab}$TrmU54 and RumA. The surface representation of RumA (**A**) and $_{Pab}$TrmU54 (**B**) is colored according to their electrostatic potential calculated with APBS (44) and presented in the same orientation as in Figure 1. The mini-rRNA substrate of RumA is shown in cartoon representation in both RumA and $_{Pab}$TrmU54. The 3′ end stem-loop is colored yellow, the 5′ end white, the target uridine 1939 green, bases 1940 and 1941 red, bases 1937 and 1938 dark blue.

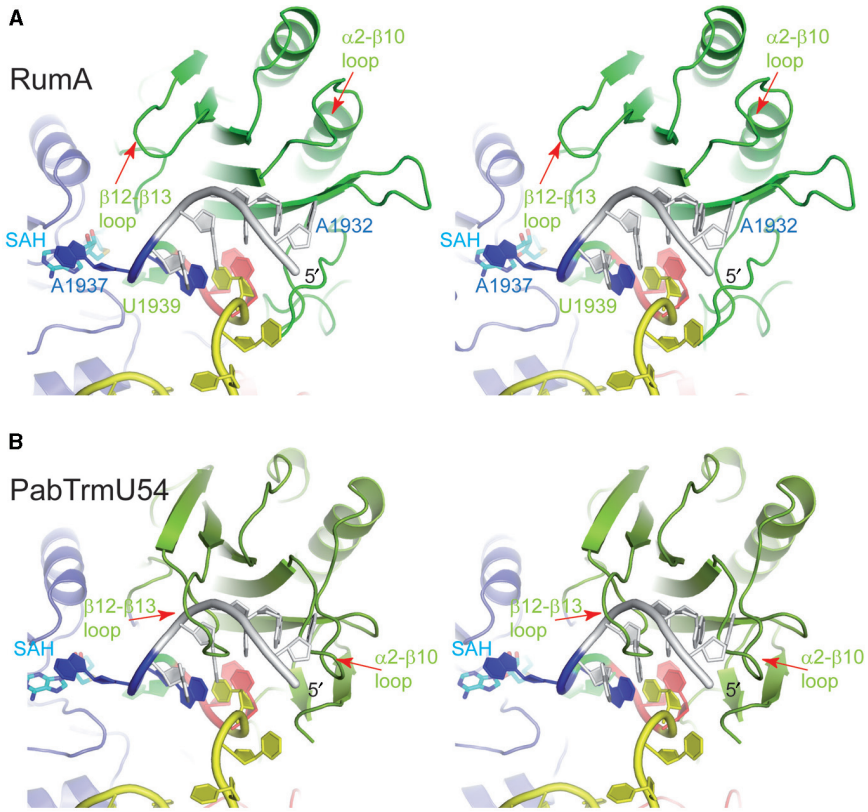

Figure 5. Recognition of the mini-rRNA by RumA and $_{Pab}$TrmU54. (**A**) Stereo representation of the recognition mode of the 5′ end of the mini-rRNA substrate by RumA. The mini-rRNA substrate is colored as in Figure 4. (**B**) Stereo representation of $_{Pab}$TrmU54 in the same orientation as A. The RumA mini-rRNA substrate is shown for comparison. The two loops α2–β10 and β12–β13 make severe steric clashes with the mini-rRNA, explaining why the latter is not a substrate of $_{Pab}$TrmU54.

Superposition of the catalytic domains of the RumA and RumA·AdoHCys·mini-rRNA structures indicates a rotation of the TRAM domain of 10° upon rRNA binding. The TRAM domain of $_{Pab}$TrmU54 also seems to be mobile, as indicated by the 5° difference in orientation between Forms I and II. The flexibility of the TRAM domain of $_{Pab}$TrmU54 is further demonstrated in crystal Form I by the higher average temperature factor of the residues in this domain (Table 1). This could be a consequence of the disorder of the β5–α1 loop connecting the central and TRAM domains (see above). Yet, the TRAM domain is less mobile in crystal Form II compared with crystal Form I because it forms more crystal contacts. The difference in orientation of the TRAM domain when the catalytic domain of Form I of $_{Pab}$TrmU54 is superimposed to that of the RumA and RumA·AdoHCys·mini-rRNA structures, is 20° and 10°, respectively (Figures 1B and 2). It is possible that this different orientation of the TRAM domain with respect to the catalytic domain compared with RumA comes from the high mobility of the TRAM domain in $_{Pab}$TrmU54. Alternatively, it may contribute to the different substrate selectivity of the two enzymes, since the TRAM domain provides numerous contacts to a hairpin segment of rRNA in the RumA·AdoHCys·mini-rRNA complex.

Superposition of the $_{Pab}$TrmU54 catalytic domains of Forms I and II also reveals that the central domains adopt different orientations, indicating intrinsic flexibility. Comparison of the free and RNA bound RumA structures shows an RNA induced reorientation of the central domain (15), with the 'hinged' motion of all three domains towards RNA resulting in the closure of the active site. Since, in $_{Pab}$TrmU54, both the TRAM and central domains are stabilized in different orientations in the two crystal forms due to differences in crystal contacts, the tRNA substrate might select the preferred protein conformation upon binding. Therefore, a conformational capture mechanism and/or an RNA induced conformational change could occur during complex formation and be involved in the specificity of the tRNA–protein interaction (32).

Modeling of the RumA mini-rRNA substrate inside the binding site of $_{Pab}$TrmU54

$_{Pab}$TrmU54 catalyzes the site-specific formation of m^5U at position 54 in tRNA. It does not methylate the *E. coli* rRNA fragment substrate of RumA that was used for the structure determination of the RumA·AdoHCys·mini-rRNA complex (data not shown) nor a similar rRNA fragment from *P. abyssi* [Figure 5 in (10)], attesting that the archaeal enzyme can discriminate between tRNA and rRNA fragment. To uncover elements that might dictate the basis of different substrate specificity in RumA and $_{Pab}$TrmU54, we first positioned the 37-mer rRNA fragment from the RumA·AdoHCys·mini-rRNA structure in the $_{Pab}$TrmU54 structure based on the

superposition of the catalytic domains (Figure 4B). This RNA is composed of two structural elements: the 5′ end containing the target nucleotide U1939 forms a compact folded loop involving several unusual intra-RNA interactions, whereas the 3′ segment is a canonical five base-paired hairpin with a seven base internal loop. Strikingly, the rRNA fragment shows remarkable complementarity with the $_{Pab}$TrmU54 surface, except for the first five residues on the 5′ end (Figures 4B and 5B). This similarity extends to the conservation of several key amino acids involved in RNA binding in RumA.

The 3′ end hairpin of mini-rRNA fits without any steric hindrance into the cleft formed at the interface between the TRAM and catalytic domains of $_{Pab}$TrmU54. In RumA, the TRAM domain makes two electrostatic contacts with the 3′ end hairpin stem through the β4–β5 loop, and numerous H-bonds, aromatic and electrostatic interactions with the 3′ end hairpin loop through the β1–β2 and β2–β3 loops (15) (Figure 2). These loops are structurally divergent in $_{Pab}$TrmU54. However, although the β4–β5 loop in $_{Pab}$TrmU54 is much shorter than that in RumA, it possesses two lysine residues (K39, K40), which may have a similar role to those that contact the 3′ end sugar phosphate backbone in RumA (K58, K59). Besides, R90 in $_{Pab}$TrmU54 may be the equivalent of R110 in the catalytic domain of RumA, which is involved in a crucial interaction with the 3′ end hairpin RNA backbone (15). Therefore, the potential interactions of $_{Pab}$TrmU54 with the 3′ end hairpin stem of mini-rRNA indicate that the $_{Pab}$TrmU54 TRAM domain contains several elements prone to bind an RNA double helix. This validates the idea that the binding mode of mini-rRNA to RumA could be used to model the binding mode of tRNA to $_{Pab}$TrmU54 (see below).

In contrast, there are no structural elements of $_{Pab}$TrmU54 that could recognize the mini-rRNA 3′ end hairpin loop similarly as in RumA. Indeed, the β1–β2 loop, which interacts with U1955 and U1956 of the RNA loop in RumA, is not conserved in $_{Pab}$TrmU54. Moreover, the β2–β3 loop of $_{Pab}$TrmU54, which is shorter and adopts a different conformation than that of RumA, does not contain any residues similar to those contacting the neighboring A1953 in RumA. This is not surprising regarding the fact that the $_{Pab}$TrmU54 tRNA substrate does not contain the equivalent of the rRNA 3′ end loop.

In the 5′ end part of mini-rRNA, the uridine at position 1939, target of the methylation in RumA, is deeply buried inside a pocket in the narrow groove between the catalytic and central domains (Figure 4A). The two conserved nucleotides (UC) following U1939 are also inserted in this groove but form only little sequence-specific interactions with the protein. In our docking of the rRNA fragment in the $_{Pab}$TrmU54 structure (Figure 4B), the three nucleotides 1939–1941 can be accommodated in a pocket of $_{Pab}$TrmU54 similar to that in RumA. Moreover, residues G89, R128, R130, H422 and R366 in RumA, which are involved in binding the sugar phosphate backbone of the 1938–1942 polynucleotide (15), are conserved in $_{Pab}$TrmU54 (respectively, G69, R108, R110, H397 and R343), which suggests a similar recognition of the backbone of this RNA fragment at the active site. Additionally, R149 in RumA, which makes hydrogen bonds to C1941, is also conserved (R123 in $_{Pab}$TrmU54), indicating a potential similar recognition of the base of C1941. Yet, since R132 in RumA, which forms hydrogen bonds to U1940 and C1942, is replaced by D112 in $_{Pab}$TrmU54, it is likely that the majority but not all the nucleotide bases near the target uridine are recognized similarly by $_{Pab}$TrmU54 and RumA.

In the RumA·AdoHCys·mini-rRNA structure, A1937 in the 5′ end rRNA fragment forms a novel-stacking interaction with AdoHCys, which is usually provided by a protein residue in other MTases. AdoHCys is bound by residues conserved between $_{Pab}$TrmU54 and RumA, with the exception of S300 in $_{Pab}$TrmU54 (G316 in RumA), which stacks on top of the AdoHCys adenine ring (Figure 3B). Such conformation, which hinders the stacking of an RNA purine base on AdoHCys, could be favored in $_{Pab}$TrmU54 in the absence of RNA. A conformational change involving stacking of the cofactor with an RNA base, as seen in the RumA structure, is not ruled out in the presence of an RNA substrate.

The last five residues at the 5′ end loop (1932–1936) clash with loops α2β1 and β12β13 of the central domain (Figure 5B) that are unique to $_{Pab}$TrmU54. This steric hindrance may probably reflect the substrate selectivity of $_{Pab}$TrmU54 because, in the RumA·AdoHCys·mini-rRNA structure, the unusual fold of the 5′ end loop of rRNA, which is mostly bound by the central domain, contributes not only to nucleotide flipping but also to substrate selectivity (15).

A mini-tRNA stem-loop is recognized by $_{Pab}$TrmU54

The activity of $_{Pab}$TrmU54 was tested using $_{Pab}$tRNA^{Asp} as substrate (10). In addition, the D stem-loop truncated tRNA^{Asp}, lacking the characteristic fold generated by the interactions between the D- and TΨC-loops was also shown to be substrate of $_{Pab}$TrmU54. Therefore, the MTase activity of the enzyme does not depend on the 3D structure of tRNA. We wanted to further determine whether the anticodon stem-loop was necessary for recognition. For this purpose, we tested here whether a mini-tRNA truncated of both the anticodon and D stem-loops (and, therefore, composed only of the TΨC stem-loop and the aminoacyl acceptor stem, which form an extended double helix) is recognized by $_{Pab}$TrmU54. $_{Pab}$TrmU54 was incubated with a 31-mer *P. abyssi* mini-tRNA substrate analog that contains 5FU at the target position (Figure 6A). According to the catalytic mechanism of RumA, C6 of a 5FU-containing RNA can form a stable covalent bond with a thiol group (C389) of the enzyme. This strategy was used to trap the covalent RumA·mini-rRNA complex for the crystal structure determination (15).

As visualized on SDS–PAGE gel after protein staining with Coomassie blue (Figure 4B), $_{Pab}$TrmU54 forms a complex with 5FU-mini-tRNA in the presence of AdoMet that migrates more slowly than free enzyme. This adduct appears to be covalent, since it is stable upon heating in SDS and on SDS–PAGE. The complex could also be detected on SDS–PAGE by ethidium bromide staining (Figure 4C), confirming the presence of RNA. These results

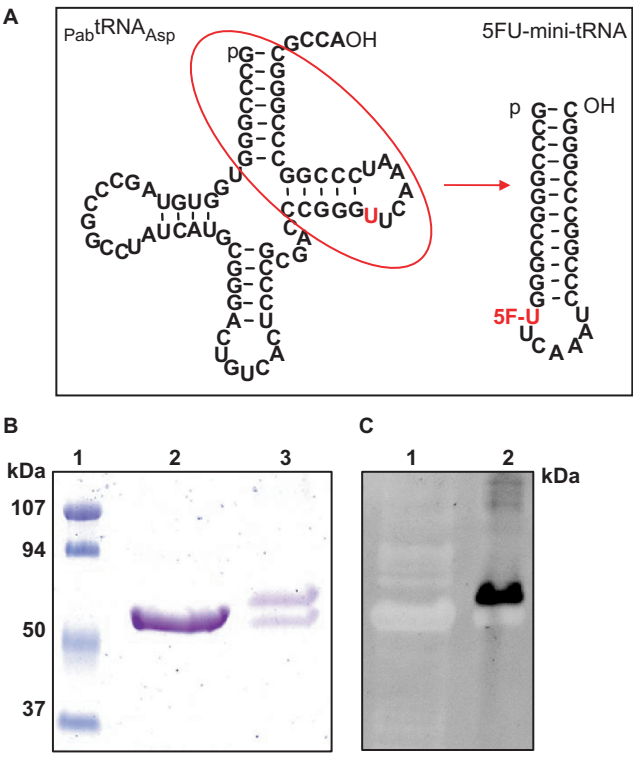

Figure 6. Formation of a covalent complex between $_{Pab}$TrmU54 and 5FU-mini-tRNA substrate analog in the presence of AdoMet. (**A**) Sequences and cloverleaf structures of *P. abyssi* tRNA^{Asp}, and 31-mer 5FU-mini-tRNA substrate analog. (**B**) SDS–PAGE analysis (10% gel) testing the formation of a covalent complex between $_{Pab}$TrmU54 and 31-mer 5FU-mini-tRNA substrate analog after Coomassie blue staining. Molecular weight markers (lane 1); 5 µg of purified $_{Pab}$TrmU54 (lane 2); incubation mixture of $_{Pab}$TrmU54 and 5FU-mini-tRNA after 2 h reaction at 50°C in the presence of AdoMet (lane 3). (**C**) SDS–PAGE analysis of the formation of the covalent complex of $_{Pab}$TrmU54 with 5FU-mini-tRNA substrate analog after ethidium bromide staining. Five microgram of purified $_{Pab}$TrmU54 (lane 1); incubation mixture of $_{Pab}$TrmU54 and 5FU-mini-RNA after 2 h reaction at 50°C in the presence of AdoMet (lane 2).

agree with the formation of a C5-methylated stable adduct with a covalent link between a thiol group of the enzyme (probably C367) and C6 of the 5FU-mini-tRNA. They also suggest the mechanism of $_{Pab}$TrmU54 is the same as that demonstrated for other (pyrimidine, C5) MTases (12,33,34).

Furthermore, we have shown that the anticodon stem-loop is not necessary for recognition of the $_{Pab}$TrmU54 target RNA, which is consistent with results previously obtained on cellular extracts of *P. furiosus* (35). Similarly, it has been shown that TrmA and Trm2p recognize a characteristic TΨC stem-loop architecture (36–39). In addition, the activity of TrmA was shown to be insensitive to the composition of the base-paired stem and the only mutation in the loop that was crucial for activity was that of C56G (37). It was concluded that the specificity of the enzyme resides rather in secondary and tertiary structural features of the TΨC stem than on the sequence. This structure, also called T-loop RNA folding motif, was identified in several other RNA structures besides tRNAs (40). It consists in a five-nucleotide motif composed of a U-turn flanked by a noncanonical base pair that confers stability to the motif, which is formed by the reverse Hoogsteen interaction between m^{5}U54 and m^{1}A58 in the case of the TΨC loop of tRNA. Different proteins may use a similar strategy for the recognition of this frequently occurring motif.

Model of the yeast tRNA^{Asp}·$_{Pab}$TrmU54 complex

We have shown above that, in $_{Pab}$TrmU54, the TRAM domain is able to bind an RNA double helix and that the D and anticodon stem-loops of the tRNA are not crucial for substrate recognition. Therefore, it is tempting to propose that the $_{Pab}$TrmU54 TRAM domain binds the aminoacyl acceptor stem of both the mini-tRNA stem-loop and the full length tRNA substrates. In this case, the TRAM domain could have a similar role to that in RumA, where binding of the TRAM domain in a RNA region distal to the target uridine was shown to provide binding energy that contributes to enhanced catalytic efficiency (15). Figure 7 shows models of $_{Pab}$TrmU54 bound to two of its substrates: the mini-tRNA stem-loop (this study) or yeast tRNA^{Asp} (10). The mini-substrate was built by deleting the D and anticodon stem-loops of yeast tRNA^{Asp} (PDB code 3TRA), which yields to a 12 bp stem and seven residues loop. It was manually positioned by superposing the aminoacyl acceptor stem with the 3′ end stem-loop of the mini-rRNA from the RumA·AdoHCys·mini-rRNA complex. In the context of the full tRNA structure, the choice of the site of interaction of the TRAM domain with the aminoacyl acceptor stem is highly constrained because some orientations lead to severe steric clashes between the protein and the D and/or anticodon stems (not shown). In a possible model of yeast tRNA^{Asp} bound to $_{Pab}$TrmU54 shown in Figure 7B, the interactions between the TRAM domain and the aminoacyl acceptor stem place the TΨC loop, with the target uridine 54, in front of the $_{Pab}$TrmU54 catalytic site, whereas the anticodon and D stem-loops show only weak interactions with the protein.

In the 3D structure of unbound tRNA, U54 is buried inside the molecule. In order to gain access to U54, the interactions between the D and TΨC stem-loops must be disrupted. Moreover, because of stacking of U54 with G53 and Ψ55 and a reverse Hoogsteen hydrogen bond with A58, the flipping of the target base has to occur. Therefore, the TΨC loop has to adopt an open conformation to make the target uridine accessible. In contrast, the m^{5}U54/m^{1}A58 interaction does not need to be disrupted in the case of *E. coli* pseudouridine synthase TruB that modifies U55 in the same tRNA region. Indeed, this enzyme recognizes the TΨC loop and accesses its substrate base without imposing dramatic conformational changes on the RNA structure (41).

Our model predicts an important conformational change in the TΨC loop in order to insert U54 in the $_{Pab}$TrmU54 active site. Base flipping alone cannot account for the insertion of the uridine in the catalytic pocket, since the surrounding bases are likely inserted in the groove between the catalytic and the central domain in a manner analogous to the RumA·AdoHCys·mini-rRNA complex because of the conservation of the amino acids that interact with the

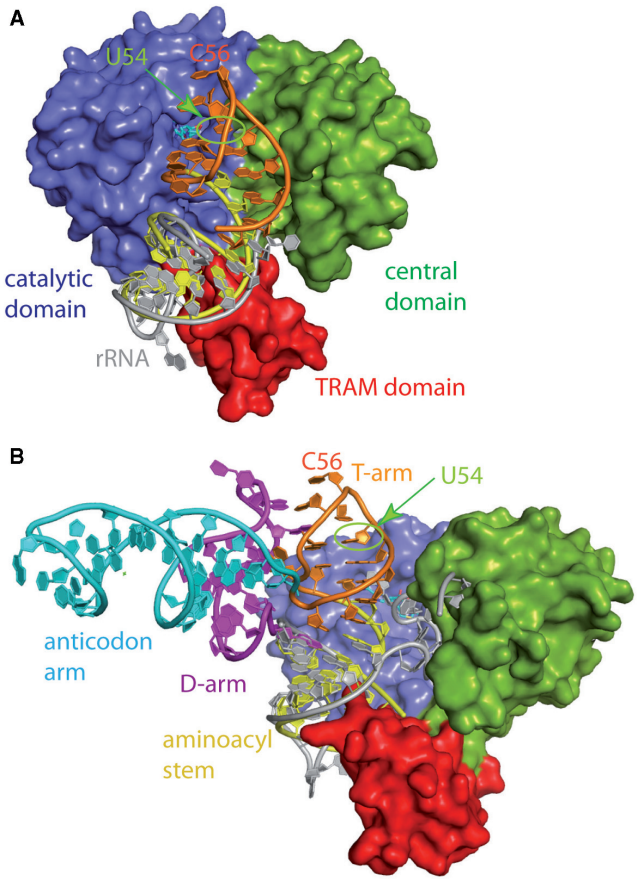

Figure 7. Docking of RNA inside the $_{Pab}$TrmU54 cleft. (**A**) Model of $_{Pab}$TrmU54 bound to mini-tRNA substrate. $_{Pab}$TrmU54 is in the same orientation as in Figure 1A. The mini-tRNA substrate was constructed by deleting the anticodon and D stem-loops of yeast tRNA^{Asp} (PDB code 3TRA). The aminoacyl stem and TΨC stem-loop are colored in yellow and orange, respectively. The mini-tRNA substrate was positioned by superposing its aminoacyl stem on the 3′ end of the mini-rRNA (in white) that was cocrystallized with RumA. (**B**) Model of yeast tRNA^{Asp} bound to $_{Pab}$TrmU54. The aminoacyl stem and TΨC stem-loop of tRNA^{Asp} are in the same position as the mini-tRNA substrate in A. The anticodon and D stem-loops are colored cyan and purple, respectively.

nucleotides nearby U1939 in RumA (see above). In our model, loops α2–β10 and α12–β13 from the central domain, which prevent the binding of the 5′ end of the mini-rRNA RumA substrate in $_{Pab}$TrmU54, are in an ideal position to recognize the TΨC loop, and possibly the anticodon stem.

Therefore, the TRAM domain might serve as a docking platform for the tRNA and act as a molecular ruler that positions the TΨC loop in the correct orientation to be remodeled by the $_{Pab}$TrmU54 specific α2–β10 and β12–β13 loops for insertion into the $_{Pab}$TrmU54 active site. As in RumA, RNA refolding probably participates in the structure specific recognition of the single target base in the RNA substrate.

CONCLUSION

The close structural similarity of archaeal $_{Pab}$TrmU54 and bacterial RumA was not necessarily expected since the two enzymes share only 23% sequence identity and act on distinct type of RNA molecules. The similar global architecture of $_{Pab}$TrmU54 and RumA, the knowledge of the RNA-binding pocket in RumA together with the surface electrostatic potential of $_{Pab}$TrmU54 were combined with experiments showing that a mini-tRNA, lacking the D and anticodon stem-loops, is recognized by $_{Pab}$TrmU54 to propose a model of yeast tRNA^{Asp} bound to $_{Pab}$TrmU54. This model indicates that it is highly probable that the TRAM domain of $_{Pab}$TrmU54 is involved in binding the aminoacyl acceptor stem of tRNA whereas the TΨC stem-loop is expected to undergo large conformational changes during catalysis so that flipping of the target uridine can occur. The specific α2–β10 and β12–β13 loops of the central domain of $_{Pab}$TrmU54 might participate in remodeling the TΨC stem-loop in order to insert U54 in the $_{Pab}$TrmU54 active site. In addition, a characteristic rearrangement of the L-shaped tRNA into the noncanonical λ-form, in which the interactions between the D- and TΨC-loops are lost (42), could also help the enzyme to efficiently access the target position. Indeed, the tRNA λ conformation exposes most of the D-arm residues in a single strand, which allows archeosine tRNA guanine transglycosylase to modify G15 in the D-loop that is otherwise buried in the L-tRNA structure (42). Simultaneously, the TΨC loop becomes exposed to the solvent, while the shape of the TΨC stem-loop is kept in the canonical L-shape. Thus, modification enzymes acting on the TΨC loop, whose activity does not depend on the canonical tertiary structure of the tRNA, could act on the λ-form tRNA. In particular, since $_{Pab}$TrmU54 does not require the L-form of tRNA [this study and (10)], the λ-form could be substrate of this enzyme. This agrees with our model, in which changing yeast tRNA^{Asp} by the λ-form of *P. horikoshii* tRNA^{Val} (PDB code 1J2B) does not create steric hindrance (data not shown). Determination of the structure of the complex of $_{Pab}$TrmU54 with an RNA substrate will provide definitive understanding about its specific recognition by the enzyme and hopefully some clues to further explain the difference of RNA specificity between RumA and $_{Pab}$TrmU54.

In the course of the submission of this manuscript, the structure of *E. coli* tRNA (uracil-54, C5)-MTase TrmA in complex with a 19-mer TΨC stem-loop was reported (43). TrmA does not possess a TRAM domain. Moreover, its RNA-binding domain does not contain an iron–sulfur cluster and has only 11% sequence identity with the central domain of RumA (Figure S1). However, the comparison of the RumA·AdoHCys·mini-rRNA and TrmA·mini-tRNA complexes indicates that both proteins have the same fold (43). Besides, the fold of the bound TΨC-loop in the TrmA complex resembles that of the uridine-containing loop of bound mini-rRNA in the catalytic core of RumA. Thus, both enzymes use a similar strategy for the recognition of RNA at the catalytic site: the refolding of the uridine-containing loops into a stacked arrangement to expose the target uridine and the following two bases, U and C, into the catalytic cleft. Moreover, the protein interactions with the RNA consensus fold (nucleotides 53–58 in TrmA) are highly conserved between TrmA and RumA. Furthermore, residues 155–158 in TrmA

(corresponding to the beginning of loop β12–β13 of $_{Pab}$TrmU54) act as a clamp that locks the TΨC stem-loop to the catalytic domain. Altogether, these results validate *a posteriori* our hypothesis that the binding mode of mini-rRNA to RumA can be used to propose a model of the $_{Pab}$TrmU54·tRNA complex and agree with our proposition that loop β12–β13 of $_{Pab}$TrmU54 is involved in the tRNA specificity of the enzyme.

SUPPLEMENTARY DATA

Supplementary Data are available at NAR Online.

ACKNOWLEDGEMENTS

We thank Marc Graille for collecting the dataset on crystal Form II, Natasa Chatziprimou for help in purifying recombinant $_{Pab}$TrmU54 protein and making first crystallization trials, Sylvie Auxilien and Djemel Hamdane for fruitful discussions and critical reading of the manuscript. H.W. was supported by a fellowship from the Association pour la Recherche sur le Cancer. Work at IBBMC was funded by BIORIB grant (BLAN07-1_194553) from the Agence Nationale de la Recherche (ANR blanche). Funding to pay the Open Access publication charges for this article was provided by the Association pour la Recherche sur le Cancer.

Conflict of interest statement. None declared.

REFERENCES

1. Rozenski,J., Crain,P.F. and McCloskey,J.A. (1999) The RNA Modification Database: 1999 update. *Nucleic Acids Res.*, **27**, 196–197.
2. Gustilo,E.M., Vendeix,F.A. and Agris,P.F. (2008) tRNA's modifications bring order to gene expression. *Curr. Opin. Microbiol.*, **11**, 134–140.
3. Helm,M. (2006) Post-transcriptional nucleotide modification and alternative folding of RNA. *Nucleic Acids Res.*, **34**, 721–733.
4. Cochella,L. and Green,R. (2005) An active role for tRNA in decoding beyond codon: anticodon pairing. *Science*, **308**, 1178–1180.
5. Agarwalla,S., Kealey,J.T., Santi,D.V. and Stroud,R.M. (2002) Characterization of the 23 S ribosomal RNA m5U1939 methyltransferase from *Escherichia coli*. *J. Biol. Chem.*, **277**, 8835–8840.
6. Madsen,C.T., Mengel-Jorgensen,J., Kirpekar,F. and Douthwaite,S. (2003) Identifying the methyltransferases for m(5)U747 and m(5)U1939 in 23S rRNA using MALDI mass spectrometry. *Nucleic Acids Res.*, **31**, 4738–4746.
7. Björk,G.R. and Isaksson,L.A. (1970) Isolation of mutants of *Escherichia coli* lacking 5-methyluracil in transfer ribonucleic acid or 1-methylguanine in ribosomal RNA. *J. Mol. Biol.*, **51**, 83–100.
8. Nordlund,M.E., Johansson,J.O., von Pawel-Rammingen,U. and Bystrom,A.S. (2000) Identification of the TRM2 gene encoding the tRNA(m5U54)methyltransferase of *Saccharomyces cerevisiae*. *RNA*, **6**, 844–860.
9. Anantharaman,V., Koonin,E.V. and Aravind,L. (2001) TRAM, a predicted RNA-binding domain, common to tRNA uracil methylation and adenine thiolation enzymes. *FEMS Microbiol. Lett.*, **197**, 215–221.
10. Urbonavicius,J., Auxilien,S., Walbott,H., Trachana,K., Golinelli-Pimpaneau,B., Brochier-Armanet,C. and Grosjean,H. (2008) Acquisition of a bacterial RumA-like tRNA(uracil-54, C5)-methyltransferase by Archae through an ancient horizontal gene transfer. *Mol. Microbiol.*, **67**, 323–335.
11. Agarwalla,S., Stroud,R.M. and Gaffney,B.J. (2004) Redox reactions of the iron-sulfur cluster in a ribosomal RNA methyltransferase, RumA: optical and EPR studies. *J. Biol. Chem.*, **279**, 34123–34129.
12. Kealey,J.T., Gu,X. and Santi,D.V. (1994) Enzymatic mechanism of tRNA (m5U54)methyltransferase. *Biochimie*, **76**, 1133–1142.
13. Urbonavicius,J., Jager,G. and Bjork,G.R. (2007) Amino acid residues of the *Escherichia coli* tRNA(m5U54)methyltransferase (TrmA) critical for stability, covalent binding of tRNA and enzymatic activity. *Nucleic Acids Res.*, **35**, 3297–3305.
14. Lee,T.T., Agarwalla,S. and Stroud,R.M. (2004) Crystal structure of RumA, an iron-sulfur cluster containing *E. coli* ribosomal RNA 5-methyluridine methyltransferase. *Structure*, **12**, 397–407.
15. Lee,T.T., Agarwalla,S. and Stroud,R.M. (2005) A unique RNA Fold in the RumA-RNA-cofactor ternary complex contributes to substrate selectivity and enzymatic function. *Cell*, **120**, 599–611.
16. Evans,P. (2006) Scaling and assessment of data quality. *Acta Crystallogr. D Biol. Crystallogr.*, **62**, 72–82.
17. Schneider,T.R. and Sheldrick,G.M. (2002) Substructure solution with SHELXD. *Acta Crystallogr. D Biol. Crystallogr.*, **58**, 1772–1779.
18. Vonrhein,C., Blanc,E., Roversi,P. and Bricogne,G. (2007) Automated structure solution with autoSHARP. *Methods Mol. Biol.*, **364**, 215–230.
19. Abrahams,J.P. and Leslie,A.G. (1996) Methods used in the structure determination of bovine mitochondrial F1 ATPase. *Acta Crystallogr. D Biol. Crystallogr.*, **52**, 30–42.
20. Perrakis,A., Morris,R. and Lamzin,V.S. (1999) Automated protein model building combined with iterative structure refinement. *Nat. Struct. Biol.*, **6**, 458–463.
21. Jones,T.A., Zou,J.Y., Cowan,S.W. and Kjeldgaard,M. (1991) Improved methods for building protein models in electron density maps and the location of errors in these models. *Acta Crystallogr. A*, **47**, 110–119.
22. Emsley,P. and Cowtan,K. (2004) Coot: model-building tools for molecular graphics. *Acta Crystallogr. D Biol. Crystallogr.*, **60**, 2126–2132.
23. Murshudov,G.N., Vagin,A.A. and Dodson,E.J. (1997) Refinement of macromolecular structures by the maximum-likelihood method. *Acta Crystallogr. D Biol. Crystallogr.*, **53**, 240–255.
24. Vagin,A. and Teplyakov,A. (2000) An approach to multi-copy search in molecular replacement. *Acta Crystallogr. D Biol. Crystallogr.*, **56**, 1622–1624.
25. Lovell,S.C., Davis,I.W., Arendall,W.B. 3rd, de Bakker,P.I., Word,J.M., Prisant,M.G., Richardson,J.S. and Richardson,D.C. (2003) Structure validation by Calpha geometry: phi, psi and Cbeta deviation. *Proteins*, **50**, 437–450.
26. Kabsch,W. (1976) A solution for the best rotation to relate two sets of vectors. *Acta Crystallogr. A*, **32**, 922–923.
27. Holm,L. and Park,J. (2000) DaliLite workbench for protein structure comparison. *Bioinformatics*, **16**, 566–567.
28. Murzin,A.G. (1993) OB(oligonucleotide/oligosaccharide binding)-fold: common structural and functional solution for non-homologous sequences. *EMBO J.*, **12**, 861–867.
29. Arcus,V. (2002) OB-fold domains: a snapshot of the evolution of sequence, structure and function. *Curr. Opin. Struct. Biol.*, **12**, 794–801.
30. Schubert,H.L., Blumenthal,R.M. and Cheng,X. (2003) Many paths to methyltransfer: a chronicle of convergence. *Trends Biochem. Sci.*, **28**, 329–335.
31. Liebert,K., Horton,J.R., Chahar,S., Orwick,M., Cheng,X. and Jeltsch,A. (2007) Two alternative conformations of S-adenosyl-L-homocysteine bound to *Escherichia coli* DNA adenine methyltransferase and the implication of conformational changes in regulating the catalytic cycle. *J. Biol. Chem.*, **282**, 22848–22855.
32. Leulliot,N. and Varani,G. (2001) Current topics in RNA-protein recognition: control of specificity and biological function through induced fit and conformational capture. *Biochemistry*, **40**, 7947–7956.
33. Liu,Y. and Santi,D.V. (2000) m5C RNA and m5C DNA methyl transferases use different cysteine residues as catalysts. *Proc. Natl Acad. Sci. USA*, **97**, 8263–8265.
34. Walbott,H., Husson,C., Auxilien,S. and Golinelli-Pimpaneau,B. (2007) Cysteine of sequence motif VI is essential for nucleophilic catalysis by yeast tRNA m5C methyltransferase. *RNA*, **13**, 967–973.

35. Constantinesco,F., Motorin,Y. and Grosjean,H. (1999) Transfer RNA modification enzymes from *Pyrococcus furiosus*: detection of the enzymatic activities in vitro. *Nucleic Acids Res.*, **27**, 1308–1315.
36. Gu,X.R. and Santi,D.V. (1991) The T-arm of tRNA is a substrate for tRNA (m5U54)-methyltransferase. *Biochemistry*, **30**, 2999–3002.
37. Gu,X., Ivanetich,K.M. and Santi,D.V. (1996) Recognition of the T-arm of tRNA by tRNA (m5U54)-methyltransferase is not sequence specific. *Biochemistry*, **35**, 11652–11659.
38. Becker,H.F., Motorin,Y., Sissler,M., Florentz,C. and Grosjean,H. (1997) Major identity determinants for enzymatic formation of ribothymidine and pseudouridine in the T psi-loop of yeast tRNAs. *J. Mol. Biol.*, **274**, 505–518.
39. Sengupta,R., Vainauskas,S., Yarian,C., Sochacka,E., Malkiewicz,A., Guenther,R.H., Koshlap,K.M. and Agris,P.F. (2000) Modified constructs of the tRNA TPsiC domain to probe substrate conformational requirements of m(1)A(58) and m(5)U(54) tRNA methyltransferases. *Nucleic Acids Res.*, **28**, 1374–1380.
40. Krasilnikov,A.S. and Mondragon,A. (2003) On the occurrence of the T-loop RNA folding motif in large RNA molecules. *RNA*, **9**, 640–643.
41. Hoang,C. and Ferre-D'Amare,A.R. (2001) Cocrystal structure of a tRNA Psi55 pseudouridine synthase: nucleotide flipping by an RNA-modifying enzyme. *Cell*, **107**, 929–939.
42. Ishitani,R., Nureki,O., Nameki,N., Okada,N., Nishimura,S. and Yokoyama,S. (2003) Alternative tertiary structure of tRNA for recognition by a posttranscriptional modification enzyme. *Cell*, **113**, 383–394.
43. Alian,A., Lee,T.T., Griner,S.L., Stroud,R.M. and Finer-Moore,J. (2008) Structure of a TrmA-RNA complex: a consensus RNA fold contributes to substrate selectivity and catalysis in m5U methyltransferases. *Proc. Natl Acad. Sci. USA*, **105**, 6876–6881.
44. Baker,N.A., Sept,D., Joseph,S., Holst,M.J. and McCammon,J.A. (2001) Electrostatics of nanosystems: application to microtubules and the ribosome. *Proc. Natl Acad. Sci. USA*, **98**, 10037–10041.

APPENDIX 1

The coordinates and structure factors of the Forms I and II of $_{Pab}$TrmU54 structure have been deposited at the Protein Data Bank (PDB codes 2jjq and 2vs1, respectively).